Lewis, O., Woolley, M., Johnson, D. E., Fletcher, J., Fenech, J., Pietrzyk, M. W., ... Gill, S. S. (2018). Maximising coverage of brain structures using controlled reflux, convection-enhanced delivery and the recessed step catheter. *Journal of Neuroscience Methods*, *308*, 337-345. https://doi.org/10.1016/j.jneumeth.2018.08.029

Maximising coverage of brain structures utilising controlled reflux, convection-enhanced delivery and the recessed step catheter

Authors: Owen Lewis[abc], Max Woolley[bc], David Johnson[bc], Julia Fletcher[c], Johnathan Fenech[c], Mariusz W.Pietrzyk[bc], Neil U. Barua[bc], Alison S. Bienemann[bc], Will Singleton[b], Sam Evans[a], Steven S. Gill[bc]

[a] School of Medical Engineering, Queen's Building, Cardiff University, The Parade, Cardiff CF24 3AA
[b] Functional Neurosurgery Research Group, University of Bristol, School of Clinical Sciences, Learning & Research Building, Southmead Hospital, UK
[c] Neurological Applications Department, Renishaw PLC, New Mills, Wotton-Under-Edge, Gloucestershire, UK GL12

Abstract

Background
The design and use of convection-enhanced delivery catheters remains an active field as failed clinical trials have highlighted suboptimal distribution as a contributory factor to the failure of those studies. Recent studies indicate limitations and challenges in achieving target coverage using conventional point source delivery.
New method
The recessed step catheter(RSC), developed by this group, does not function as a point source delivery device, but instead utilises 'controlled reflux' of the infusate to a flow inhibiting recess feature. Here we investigate a range of clinically useful step lengths in agarose gel and investigate proof-of-principle *in vivo*(n=5). Infusion morphology was characterised in terms of length, width and distribution volume over a range of flow rates.
Results
Increases in catheter step length strongly correlated with increased infusion volume and length ($r>0.90, p<0.001$) while small but significant reductions of infusion width were recorded($r<-0.62, p<0.001$). Step lengths below 6mm produced spherical infusion clouds while steps above 12mm produced elongated infusions. Increasing peak flow rates resulted in significant reductions in coverage at each step length, and increased risk of reflux beyond the step. Modifications to the infusion morphology using changes in step length were confirmed *in vivo*.
Conclusions
The RSC can be tailored to each patient's unique anatomical requirements to maximise coverage and optimise distribution in targeted neurological structures. Loss mechanisms *in vivo* remain "real-world" challenges for all devices, but the combination of recess and variable catheter step length provide a simple mechanism for controlling the infusion morphology and maximising coverage for neurological indications.

Key words

Convection-Enhanced Delivery, Recessed-step-catheter, Parkinson's Disease, CED, PD, controlled reflux

Highlights

- The recessed step catheter can be used to bypass the blood brain barrier in neurodegenerative or neuro-oncological indications to deliver therapeutics directly to target tissues
- The variable step length can be used to control the infusion morphology in convection-enhanced delivery infusions to match target structures
- Novel surgical trajectories could be employed to maximise coverage of neuroanatomical targets such as the striatum, thalamus or pons

Corresponding author: Owen Lewis, School of Medical Engineering, Queen's Buildings, The Parade, Cardiff CF24 3AA
lewisto1@cardiff.ac.uk

1 Introduction

Systemic routes of administration for macromolecules targeting neurological conditions have significant limitations for achieving therapeutic drug concentrations within the central nervous system (CNS). Transportation from the blood stream to neurological tissues is severely limited because of the blood brain barrier (Stockwell et al. 2013). Direct delivery via a series of intracranially implanted catheters offers a promising alternative to this route as expensive or toxic substances can be administered at much lower doses than would be required systemically to achieve the same local concentration. It also allows drugs to be delivered to specific targeted tissues, and not widespread throughout the CNS.

Convection-Enhanced Delivery (CED) is an infusion methodology which utilises implanted catheters to increase local hydrostatic pressures at the site of infusion to mimic vasogenic oedema (Bobo et al. 1994). Infusion concentrations are elevated above that which could be achieved via diffusion alone, as the random path of diffusive molecules would take days/weeks to reach a similar distance from the site of infusion (Saltzman 2001).

Despite initial description of the technique being published in 1994 no clinically available treatment utilising CED is currently available outside of investigational clinical trials, indicating the difficulty of translation from lab and pre-clinical trials into the clinic (Gill et al. 2003; Lang et al. 2006; Kunwar et al. 2010; Mueller et al. 2011; Warren Olanow et al. 2015).

While higher than average placebo responses are a known phenomenon in neurological studies (Goetz et al. 2008; Kunwar et al. 2010), cited among the reasons for failure of these studies was the requirement for increased experience of the users, improved equipment and predictability of implanted devices.

The incorporation of distribution predictions within the planning stage of neurosurgical procedures has been advocated and will no doubt provide a step change towards improved trial outcomes (Raghavan et al. 2016). Underpinning such algorithms however must be an empirical knowledge of how each device

performs. While not the only devices used for direct delivery, End Port Catheters (EPC) are often described as having an idealised, spherical distribution pattern which emanates from their tips (Ivanchenko et al. 2010). Investigations using devices with this aim have shown that this use is suboptimal in that multiple payloads are often required to deliver clinically meaningful infusion volumes (Bartus et al. 2013; Sillay et al. 2013). This increases the duration of the infusions but also the complexity of the implant as the device must be moved multiple times throughout a treatment. Further, anatomical structures of interest for some neurodegenerative pathologies, such as the putamen and caudate nucleus are themselves, not spherical but elongate. Despite axial trajectories for foetal cell deposition being described in 1995 (Breeze et al. 1995), implantation (Brady et al. 2013; Bankiewicz et al. 2016) likely due to the surgical and anaesthetic challenges of implantation and extended infusions associated with keeping patients in the prone position to access the long axis of targets such as the caudate nucleus or the putamen.

We developed a fully polymeric catheter device which utilises image guided, robot assisted implantation remote from an MRI suite (Barua et al. 2013a; Gill et al. 2013; Lewis 2015) enabling implantation along almost any desired trajectory. Once implanted, real time scans are possible to track and optimise the infusion regimes. The recessed step catheter does not function as a point source distribution device but one that utilises a form of "controlled reflux" (Woolley et al. 2013; Singleton et al. 2017). As the recess forms an inhibiting feature, fluid flows from the tip of the device around the boundary to the recess (along the catheter to the outer guide tube, defining the *step length – see* Figure 1), providing a potential mechanism for higher overall coverage in target structures within a single implantation procedure. The use and optimisation of chronically implanted catheters are however little known and further research is required for optimisation (Lewis et al. 2016). Here we investigate and characterise the variable step length feature of the recessed step catheter to optimise the morphology of infusions as a means of maximising coverage of neuro-anatomical structures.

2 Materials and Methods

2.1 *In vitro* evaluation

2.1.1 Agarose gel and infusate preparation

Agarose gel (0.6%) was prepared by mixing molecular grade agarose gel (Severn Biotech LTD, UK) with concentrated Tris Borate-ETDA buffer (Severn Biotech, UK) and deionised water. The mixture was heated in a microwave for 5minutes, stirred and then heated further until all powder had fully dissolved. The heated solution was decanted into 50x50x150 clear, rectangular acrylic containers (Volume:375ml) and left to cool and solidify to room temperature.

A 3mm acrylic lid was secured to the pot and used to simulate the skull, allowing the recessed step catheter to be press fit into the acrylic plate, mimicking the implantation procedure.

Trypan Blue powder (Sigma Aldrich®) was weighted and dissolved in deionised water to a concentration of 0.4% and used as a high visual contrast infusate.

2.1.2 Catheter

Recessed Step Catheters (neuro|infuse™, Renishaw PLC, UK) are formed in three parts using an Outer Guide Tube (OGT), Inner Guide Tube (IGT) and a sub-millimetre diameter catheter (Gill et al. 2013; Lewis 2015). The device was prepared by cutting an OGT to 60mm and the IGT to 58.5mm creating a 1.5mm recess. Catheters were cut at lengths of 63, 66, 72, 78mm, creating step lengths of 3, 6, 12 and 18mm beyond the OGT.

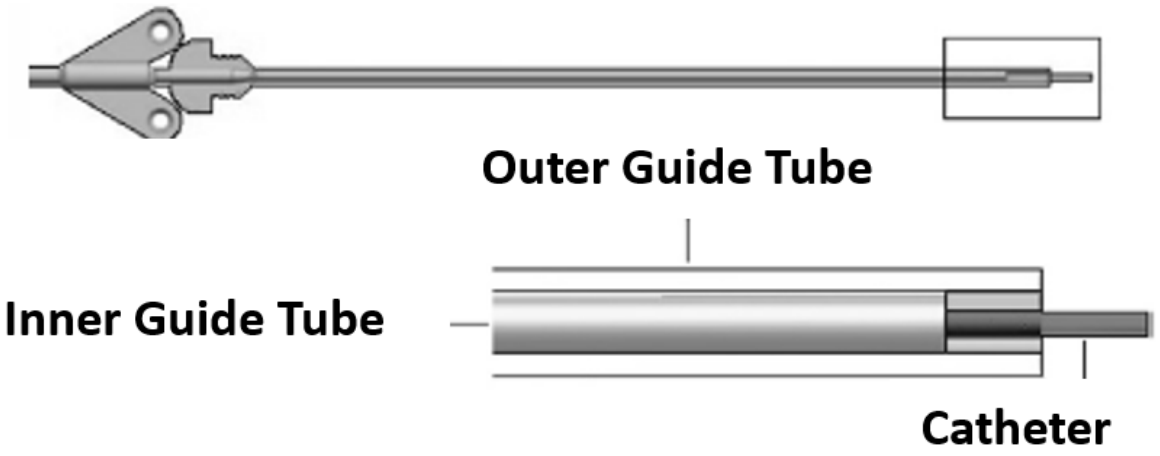

Figure 1; Fully implantable recessed step catheter assembly, inset showing a cut away view of the tubing and the formation of the recess

2.1.3 Delivery tooling

As a polymeric device, each of the guide tube elements must be delivered over delivery rods to ensure they maintain target accuracy. The OGT is delivered over a tungsten carbide delivery rod and held just short of the final implantation position. The OGT is then advanced over the rod to create a tissue/ gel plug in the base of the assembly. The IGT is then passed over a steel rod while aspiration is used to minimise the introduction of air into the infusion area.

A 0.6mm diameter rod, is then used to penetrate the gel beyond the OGT to the depth of the catheter, creating a track for the unsupported catheter to maintain target accuracy.

2.1.4 Test set up

Agarose pots were held in a bespoke fixation rig (Figure 2). A human stereotactic frame (Radionics® CRW™, Integra Lifesciences Corp.) was used to aid delivery of guide rods and catheter elements into the gel. A DSLR camera (Model 1200D, Canon Inc) was attached to a laptop fitted with Digital Photo Professional (Canon, Inc) remote shooting software. Additional lighting was used as required to illuminate the infusion. B|Braun™ Perfusor Space syringe pumps were used to run *ramp and taper* infusion regimes (Figure 3).

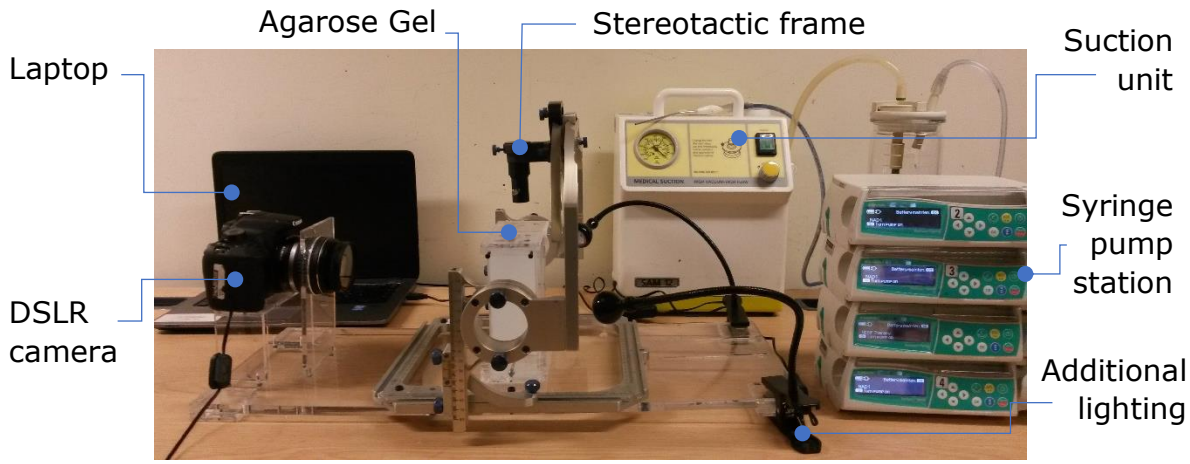

Figure 2; Schematic of gel infusion test set up

2.1.5 Infusion volume and regime

A retrospective study of anonymised surgical plans from a backlist of some of the authors historical Deep Brain Stimulation (DBS) cases was performed to establish baseline volumes of two likely neurodegenerative target structures, the putamen and caudate nucleus. 143 Parkinson's disease patients were analysed using an auto-segmentation tool (within Renishaw's neuroinspire™ surgical planning software) for anatomical structures

Average putamen volumes were 4.30±0.03ml (range: 2.89-5.94ml) which compares favourably to a smaller study conducted using only 11 cases (Yin et al. 2009)

Average caudate nucleus volumes were 2.90± 0.03ml (range 2.03-4.64ml) which was similar to previously published data from the same source.

Interstitial space in grey matter accounts for ~20% of the volume fraction (Roitbak and Sykova 1999), published values for infusions into the rat striatum confirm a V_d/V_i ratio of 5±0.2 (mean ± standard deviation)(Chen et al. 1999).

Targeting complete coverage of the average putamen would therefore require an infusion volume of at least 0.8ml (800µl), or 0.4ml (400µl) split over 2 catheters.

Slowly increasing the interstitial pressure at the target site by stepping or ramping the infusion rate from low to high minimises the risk of overwhelming inhibition features such as a step or recesses (Bankiewicz et al. 2000; Bienemann et al. 2012; Barua et al. 2013b; Gill et al. 2013).

Syringe pumps (Perfusor® Space, B|Braun) were programmed with three linear ramp and taper profiles delivering a fixed infusion volume of 400µl, ramping from zero to the peak flow rate (Q) over 40mins (Figure 3). Total infusion times were 1hr (Q=0.6ml/hr[10µl/min]), 1hr40mins (Q=0.3ml/hr[5µl/min]) and 4hrs21mins (Q=0.1ml/hr[1.3µl/min]) which were all considered clinically translatable.

A minimum of 9 repeats for each step length at each flow rate were performed (n=108).

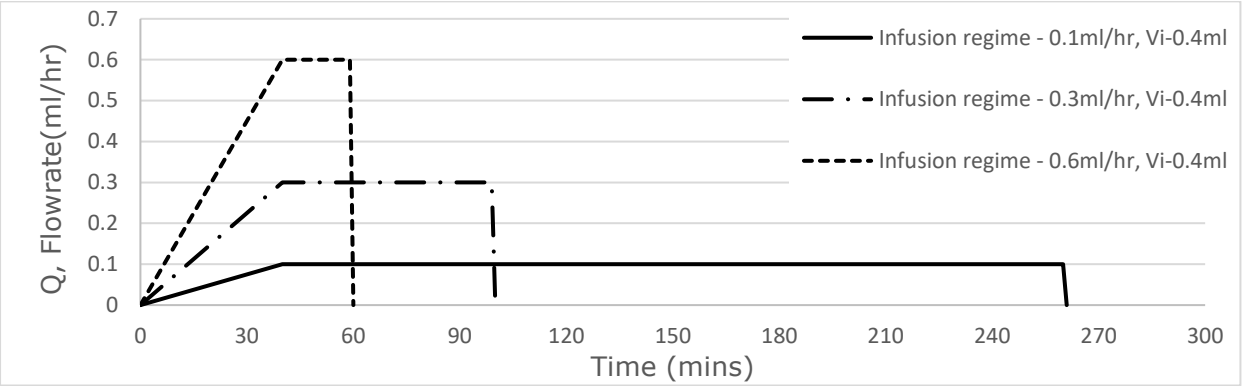

Figure 3; Investigational, clinically translatable infusion regimes for intermittent delivery

2.1.6 Infusion image acquisition rig

Following completion of the infusion (<10mins) the agarose gels were emptied into a bespoke cutting matrix. 150mm long skin grafting blades (Swann Morton) were used to section the gel into 3mm slices. Slices containing the midline of the infusion cloud were laid onto a graduated platform (Figure 4). Compressive distortions were minimised as the gel was smoothed to the known cross-sectional dimensions. A diffusion light box was placed over the rig prior to image acquisition with a Canon camera (described above) to provide uniform and consistent lighting of the samples.

Images of the infused gel were recorded within approximately 10minutes following completion of the infusion to minimise diffusion effects.

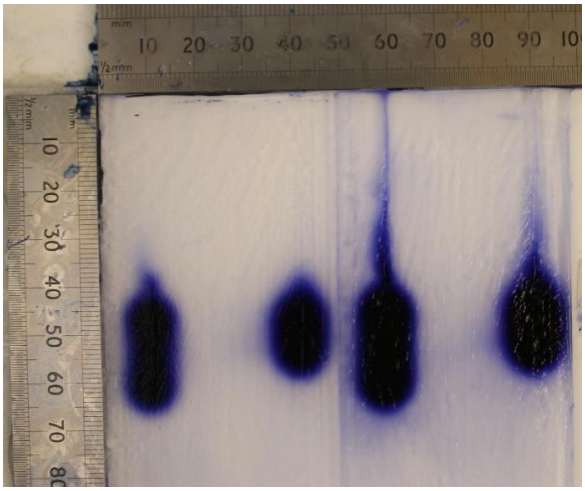

Figure 4; infusion imaging rig showing well demarcated infusion clouds within 3mm thick slices of agarose gel against a graduated border

2.1.7 Image analysis

Images were loaded into the image segmentation toolbox of Matlab 9.2 (The Mathworks, Inc., Natick, Massachusetts, United States). Infusion areas were magnified to fill the screen and the manual polygon plotter tool used to profile the boundary of the infusion, creating a segmented binary image with the same dimensions as the base image. The binary image was exported to the

workspace. Pixel width was calibrated for each image using the inbuilt steel rules which formed part of the imaging rig. Infusion Distribution Volume (V_d) was calculated on a pixel line basis as a cylindrical volume; Infusion width was halved, creating a radius while the height was the calibrated pixel height. Calculations were repeated for each line and the sum total provided the V_d. Maximum infusion length and width were also recorded.

Sectioned gel slices displayed a clear profile boundary for the infusions as a dark, saturated core with a weaker, diffuse boundary. The band of diffuse infusate was routinely 1-2mm in width and inherently variable, to minimise subjectivity, the manual profiles were created for each infusion at the border of the highly saturated core region. Analysed volumes are therefore likely to underestimate total coverage but provide a more direct comparison between tests.

2.2 *In vivo* evaluation

2.2.1 Surgical procedures

Surgical procedures were performed in accordance with the Animals (Scientific Procedures) Act (1986) under specific UK Home Office project and personal licence (project licence number 30/2909) at a licensed establishment. Study protocols were pre-approved by the University of Bristol Ethical Review board. Bilateral infusions into the grey matter (putamen or thalamus) of 5 large white landrace pigs were conducted using the recessed step catheter (n=12 infusions). Outer guide tubes were placed within the boundary of the target structure and the catheter tip was implanted to sufficient depth to create a series of increasing step lengths to a maximum of 12mm (restricted by the size of the thalamus in the porcine model).

Anaesthesia, head fixation, MRI scanning and stereotactic procedures were performed as previously described (White et al. 2011; Barua et al. 2013c).

2.2.2 Test infusions

Artificial cerebrospinal fluid (aCSF) was prepared with a 2mM concentration of gadolinium based contrast agent (GBCA), Magnevist™ (Bayer) and loaded into a fixed volume reservoir. Infusion volumes to the putamen were typically 120µl while infusions into the larger thalamus were typically 200µl.

Real time (sequential T1 weighted) MRI scans were performed by placing the fixed volume reservoirs downstream of 6m access lines which could extend into the bore of the scanner, allowing the infusion pumps to remain in the control room. Ramped infusion regimes were used as described above with flow rates peaking at 0.18-0.3ml/hr.

2.3 Statistical analysis

Sample groups larger than 2 were analysed using a one-way ANOVA to establish statistically significant differences in mean populations of V_d, infusion width and length between flow rates and between step lengths.

Pearson correlation coefficients were calculated for the distribution volume, width and length at each infusion flow rate over the step length groups (Field 2007).

3 Results

3.1 *In vitro* infusion morphology: Infusion length and width

In the gel model, as expected, there was a very strong correlation between increased step length (SL) and increased infusion length (Figure 5a: Q1[r=0.95, p<0.001], Q5[r= 0.98, p<0.001], Q10[r=0.98, p<0.001]) as infusions refluxed to the flow inhibiting feature. Increasing the infusion length also resulted in a numerically small but significant drop in the maximum infusion width at each step length (Figure 5b: Q1[r=-0.89, p<0.001], Q5[r=-0.83, p<0.001], Q10[r=-0.60, p<0.001]).

Average distribution lengths were significantly reduced when increasing the infusion flow rate (Q) at each of the step lengths investigated (SL(3mm); $F(2,27)=31.6$, $p<0.001$, SL(6mm); $F(2,29)=25.3$, $p<0.001$, SL(12mm); $F(2,30)=19.7$, $p<0.001$, SL(18mm); $F(2,29)=9.5$, $p<0.001$). Average distribution width was also significantly reduced when increasing the infusion flow rate (Q) at each of the step lengths investigated (SL(3mm); $F(2,27)=116.0$, $p<0.001$, SL(6mm); $F(2,29)=49.9$, $p<0.001$, SL(12mm); $F(2,30)=75.2$, $p<0.001$, SL(18mm); $F(2,29)=46.8$, $p<0.001$).

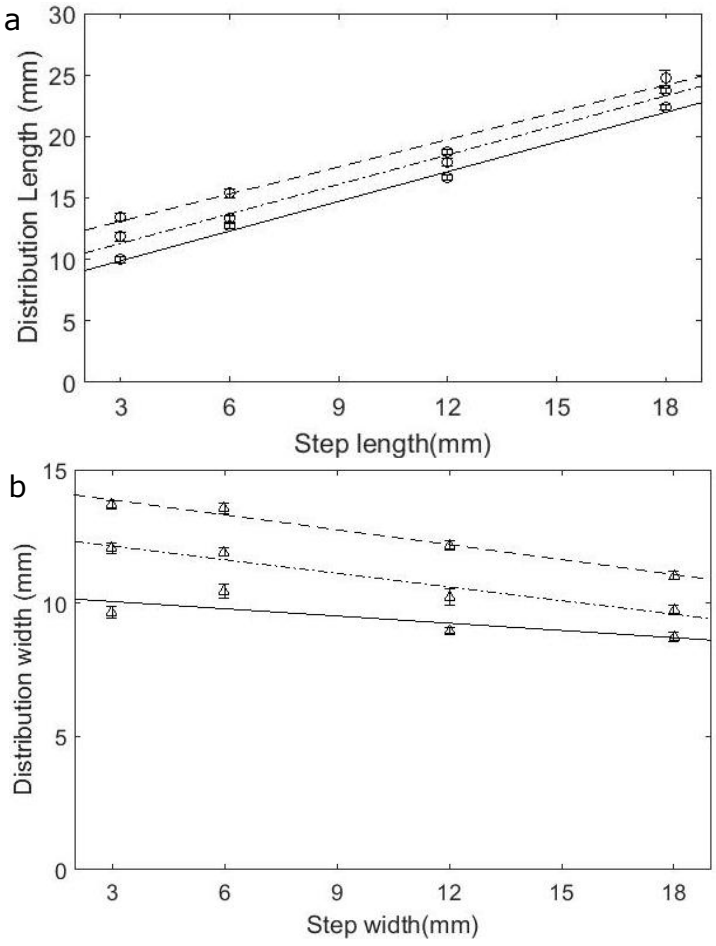

Figure 5; a) Q1 (top), Q5 (middle) and Q10 (bottom) trendlines for distribution length versus step length, b) Q1 (top), Q5 (middle) and Q10 (bottom) trendlines for distribution width versus step length

3.2 *In vitro* infusion morphology: Distribution volume

Increasing the RSC step length resulted in a significant increase in the volume covered across all infusion flow rates tested (Q1[r=0.66, p<0.001], Q5[r=0.74, p<0.001], Q10[r=0.78, p<0.001]). Average distribution volumes were analysed immediately after the completion of the infusion. Vd was significantly reduced when the infusion flow rate (Q) at each step length was increased (SL(3mm); F(2,27)= 71.3, p<0.001, SL(6mm); F(2,29)= 65.4, p<0.001, SL(12mm); F(2,30)= 103.6, p<0.001, SL(18mm); F(2,29)= 69.4, p<0.001) (Figure 6).

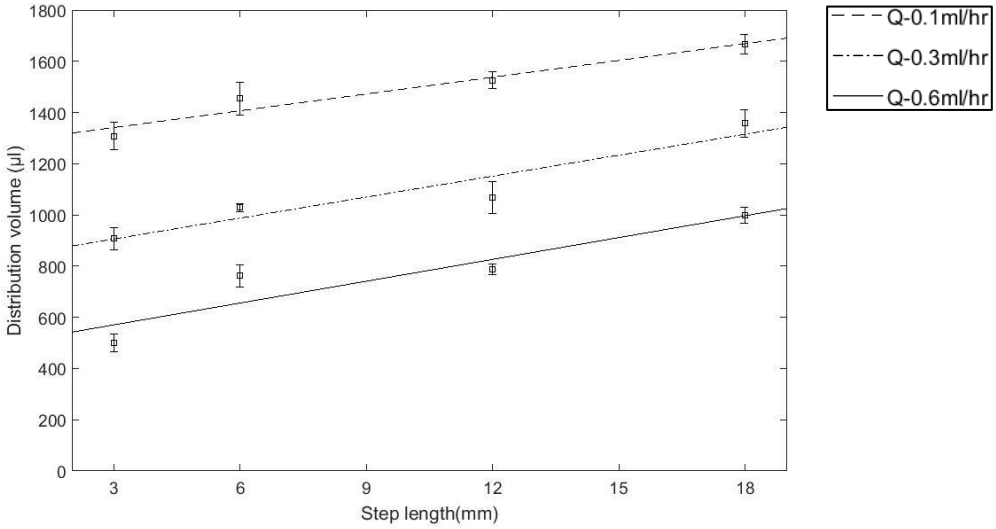

Figure 6; Q1 (top), Q5 (middle) and Q10 (bottom) trendlines for distribution volumes versus step length

3.3 *In vivo* infusion morphology: Length and width

In vivo infusions were grouped into two volumes; 120µl for the putamen and 200µl for the thalamus. Infusions into the porcine grey matter show a strong correlation for a linear rise of infusion length as the catheter step length is increased (Vi(120µl):R=0.90, p=0.006, Vi(200µl):R=0.84, p=0.03) (Figure 7a). While the infusion widths reduce in both infusion volumes, the magnitude of the change is non-significant in the putamen (Vi(120µl):R=-0.62, p=0.13, Vi(200µl):R=-0.82, p=0.05)(Figure 7b).

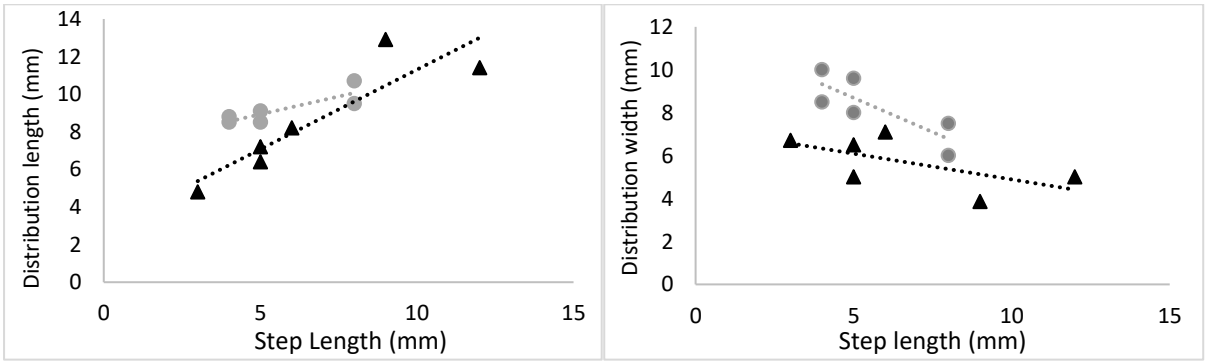

a) b)

Figure 7; a) Length of infusions achieved in the porcine grey matter; triangles=120µl (at 5µl/min), circles = 200µl (at 3µl/min); b) width of infusions achieved in the porcine white matter; triangles=120µl (at 5µl/min), circles = 200µl (at 3µl/min)

As the 120µl infusions reached a slightly higher peak flow rate of 0.3ml/hr, a shorter infusion length and smaller width may be anticipated in line with the results of the gel experiments. All infusions refluxed back to the inhibiting step in a predicable fashion across all lengths tested (3-12mm) (Figure 8a-d).

3.4 *In vivo* infusion morphology: distribution

All infusions showed small numerical increases in coverage as the step length increased, but failed to show significance (Vi(120µl):R=0.77, p=0.27, Vi(200µl):R=0.77, p=0.07) (Figure 8e).

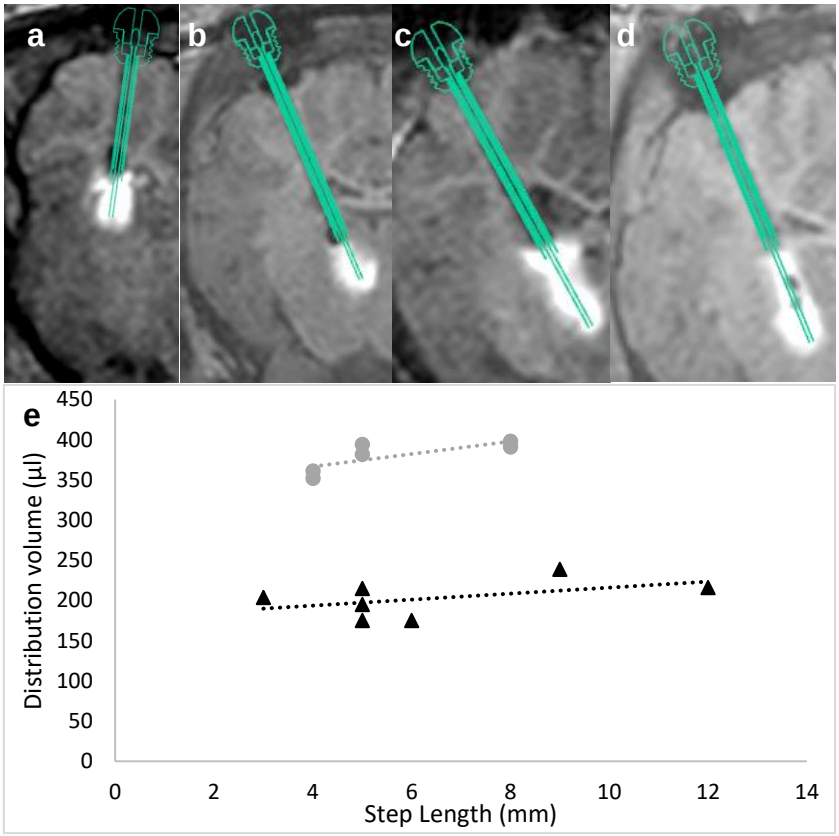

Figure 8; in vivo MRI scans of infusions using the recessed step catheter in the porcine model - a) 5mmstep, b) 6mm step, c) 8mm step, d) 12mm step, e) distribution volume achieved from infusions into the porcine grey matter; triangles=120µl (at 0.3ml/hr) circles = 200µl (at 0.18ml/hr)

4 Discussion

4.1 Controlled reflux

The catheter was implanted under a pressure head, provided by the infusion pump to minimise the inclusion of tissue/ gel into the distal tip of the catheter. Infusions were run using a stepped or ramped profile to minimise the pressure local to the catheter tip upon initial release of the internal line pressure. The initial reflux was instantaneous, passing from the tip of the catheter immediately to the recessed step (Figure 9b). Once flow was retarded below the step, a stable pressure region is believed to establish and fluid flow pathways were

initiated radially along the step region (Figure 9c-e). Convection continued until a critical point is reached where local pressures required to continue infusions radially from the step, exceed those provided by the flow inhibitor and secondary reflux commences around the outer guide tube (Figure 9f).

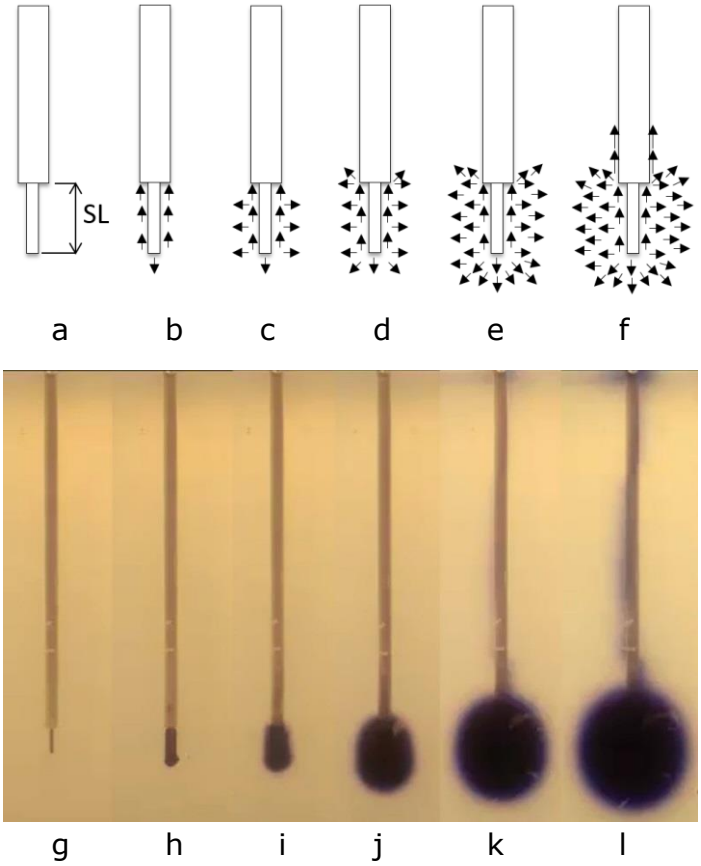

Figure 9; The stages of controlled reflux; a) implanted device – SL=Step Length, b) initial reflux, c) ramped/ stepped increase in the flow rate leading to containment of flow front at the inhibition feature and establishment of lateral flow pathways, d) peak flow rate achieved and stable convection reached, e) optimal limit of delivery, f) overload – pressure exceeds inhibition feature limit

4.2 Controlling infusion morphology

The increase of backflow with increases in catheter diameter and infusion flow rate are by now, well-known phenomena (Chen et al. 1999). Controlled reflux (Woolley et al. 2013) is therefore attained by embracing this inevitable event and restricting it below a flow inhibiting feature (Figure 1 and Figure 9). The first evidence of a recessed step was previously described by this group (Gill et al. 2013). Unlike monolithic alternatives however, the recessed step catheter can be cut and assembled based on patient data giving a fully analogue step length. Here we investigated the modification of the step length beyond the previously utilised standard of 3mm (Krauze et al. 2005; Gill et al. 2013). This investigation in the gel model has identified the predictable behaviour of the RSC to create infusions with increasing lengths in a robust way, utilising controlled reflux (Figure 10a-b) which could be used to maximise coverage of pre-clinical or human neurological structures.

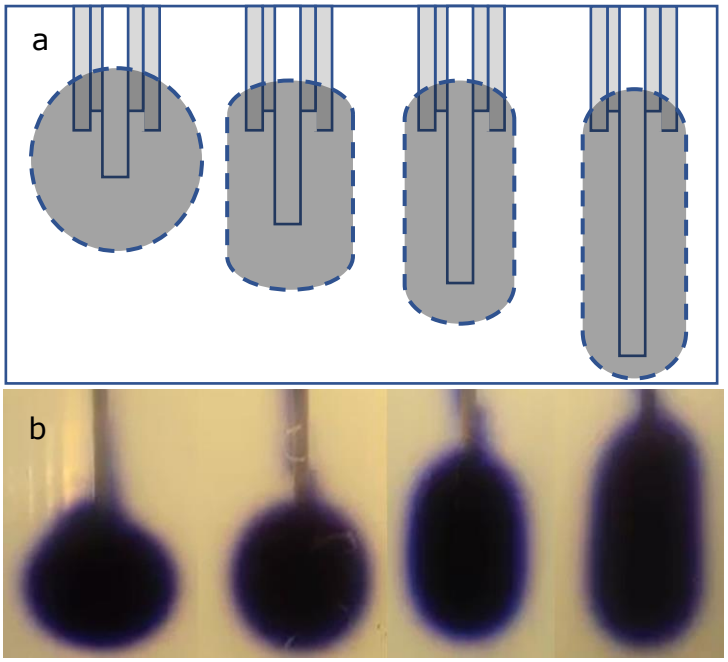

Figure 10; a) Schematic of infusion morphology characteristics associated with increasing the step length of the recessed step catheter, b) actual infusions associated with increasing step lengths

Unlike point source delivery devices, the RSC infusion cloud length closely matches that of the step length. Conversely and logically, the longer infusion clouds which share a fixed input volume, narrowed as a consequence, limiting lateral coverage which is typical of point source CED infusions. Less obvious was the reduction in coverage volumes which resulted from infusions into short step length assemblies. With an infusion volume (V_i) of 400µl for each experiment, a distribution volume (V_d) between 1600-2000µl may have been anticipated given a V_d/V_i ratio of 4:1-5:1. The mean infusion volumes recorded here range from 550-1700µl. As spherical infusions must convect to a larger radial distance than infusions spread over the region of a longer step length, spherical infusions must have higher concentration cores at the end of an infusion.

These characteristic profiles identified in the gels were also observed *in vivo*, with infusate refluxing in a controlled manner to the step before stabilising and distributing laterally. As might be expected, infusions into live tissues are less uniform than in homogenous gels however linear increases in infusion cloud length and a reduction in width were observed across the small number of catheters tested which demonstrates proof of principle.

We observed that secondary reflux occurred most often in tests utilising short step lengths (3-6mm) and the highest flow rate (0.6ml/hr). This may help explain the difficulty in directly translating pre-clinical results to clinic, as smaller infusion volumes would typically be infused to cope with the smaller anatomy of, for example, rodent, porcine and primate models, resulting in less reflux. Generally, faster flow rates are regarded as more desirable in human applications as shorter infusions are more cost effective and preferred by both clinicians and patients (Bankiewicz et al. 2016). It is of interest to note therefore that the trends observed in this study indicate that faster rates are associated with smaller distributions at the end of the infusion and increased rates of

undesirable reflux. It is noteworthy that the infusion duration at 0.1ml/hr takes more than 3hrs longer than at 0.6ml/hr providing more time for fluid pathways to develop in the substrate. High concentration gradients will of course continue to distribute after the end of the infusion, but through the action of residual pressure and diffusion alone. *In vivo*, such action would be subject to loss mechanisms (e.g. metabolism, drug half-life, perivascular losses and cerebrospinal fluid turnover). High concentration, homogenous coverage of a large area is therefore of primary interest. A compromise must therefore be struck between the preferred, short infusion times resulting in smaller distribution volumes, or longer infusion times that provide greater coverage, reduced risk of reflux but greater risk of unavoidable losses via natural clearance mechanisms.

As previously discussed, maximising coverage of target structures can be better achieved if the infusion morphology more closely matches that of the target. Dividing the length to the width of each infusion respectively, normalises the distribution morphology in to two distinct types; Spherical and Cylindrical.

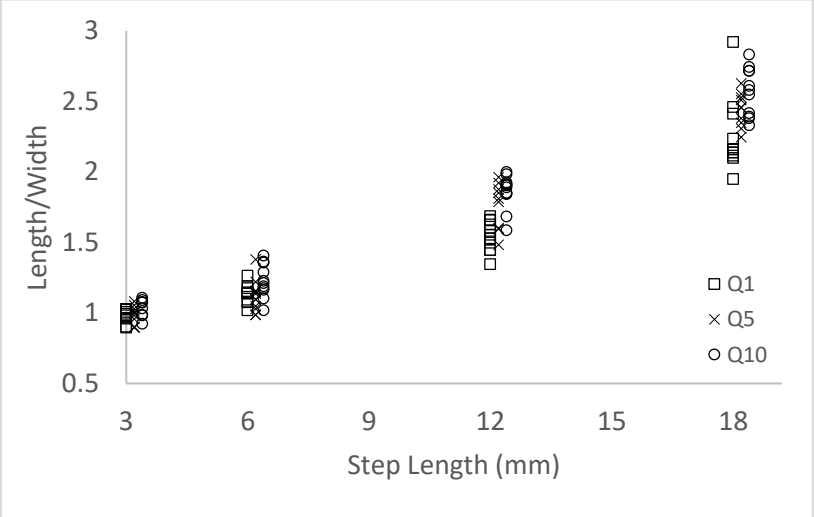

Figure 11; Infusion morphology aspect ratio

The shorter step lengths, 3 and 6mm, produce a spherical like infusion with a length/width ratio of 1:1 to 1:1.5 (for comparable, clinically relevant infusion volumes), which would account for the point source distributions historically expected from CED devices. Increasing the step length above 12mm resulted in infusion aspect ratios of 2:1 or 3:1 (Figure 11).

Application of the RSC characteristics to clinical indications would see safe trajectories being chosen based on maximising the catheter step length within the target structure, providing patient specific opportunities to maximise target coverage. While *in vivo* loss pathways, clearing mechanisms and reflux remain real world challenges, this basic empirical model of infusion morphologies can provide a useful tool when planning catheter implantation targets and trajectories.

Spherical infusions may continue to suit targets such as the pons or thalamus while elongate, cylindrical infusions would match structures like the putamen,

caudate nucleus or hippocampus (etc.). This may be over simplistic however, as the target tissue volume is not homogeneously distributed throughout structures like the putamen. The anterior aspect of the putamen is wider and taller than in the posterior of the structure. Preferential surgical planning strategies may combine the placement of a shorter stepped catheter vertically, down into the anterior portion while further catheters with much longer steps could be placed along the long, midline axis of the structure, from an anterior or posterior approach (e.g. Figure 12).

Figure 12; Example a drug delivery surgical plan within neuro|inspire™ (Renishaw plc, UK) that may maximise structure coverage

4.3 Intervening in refluxing infusions

As described above, we observed secondary reflux at the highest frequency in experiments with short step lengths and high flow rates. Once a reflux pathway has developed large volumes are continually lost down this path of least resistance.

As an additional investigational endpoint, we investigated the ability of the user to halt reflux as it became visible in the gel model. Twelve infusions were performed using 3, 6 and 12mm steps with infusions ramped to the fastest flow rate (0.6ml/hr) in 40mins. Secondary reflux occurred routinely within the first 30mins after initiating the infusion (Figure 13 a-f), which may account in part for the lower distributions seen. Once observed, the user intervened in the infusion regime, dropping the infusion rate to 0.1ml/hr or initiating a new ramp profile to 0.1ml/hr. In both cases the secondary reflux was halted at the initially observed

level and the remaining infusion volume continued to develop as desired below the recessed step (Figure 13 g-l).

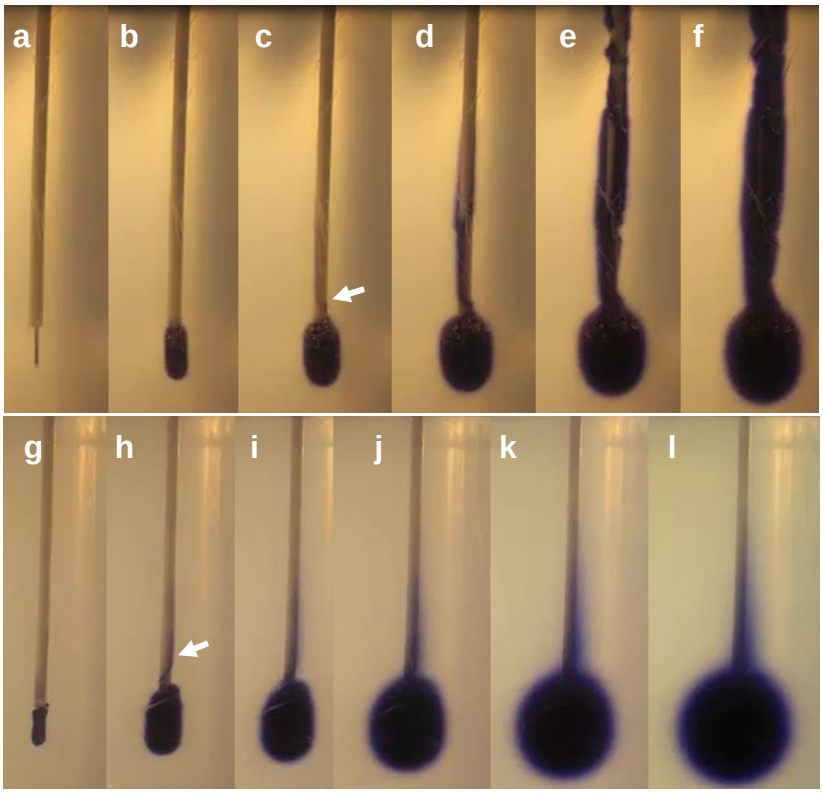

Figure 13; Progression of infusions: a-f) standard 40minute ramp run to peak rate of 0.6ml/hr (arrow indicates initiation of visible secondary reflux), g-l) standard 40minute ramp run to peak rate of 0.6ml/hr halted and dropped to lower rate after visible reflux begins

Our preliminary investigations suggest that priming the flow pathways ahead of increasing flow rates may yield favourable outcomes but further work is required to optimise this paradigm. As there is inherent variability within neurodegenerative populations our investigations would discourage the use of a *"one size fits all"* approach, and real time or post-infusion imaging would augment a treatment regime which enables the clinician to "drive" the implanted system based on real feedback. Implanted catheters could then be optimised with initial infusion parameters, but fully implanted MRI compatible systems also offer the ability to maintain long term performance through periodic test infusions.

5 Conclusions

We have demonstrated how the recessed step catheter can be used to control the morphology of infusates within an idealised, homogeneous gel model and demonstrated proof of this principle *in vivo* in porcine grey matter structures.

The drive towards ever faster flow rates to minimise clinical time must be balanced against the increased risk of losses due to reflux and reduced distribution volumes. Further work is required to investigate optimal infusion regimes for minimising reflux.

Real time or post-infusion imaging offers users the opportunity to fine tune infusion regimes, as we have demonstrated that reducing infusion rates can offer improved distribution volumes and an opportunity to actively control infusion morphology. Real time or post infusion imaging therefore remains critical to CED treatments in order to optimise distributions in an inherently variable patient population. A fully MRI compatible implant will enable periodic infusion modulation to maximise coverage in the desired target anatomy over time or optimise catheters placed in unavoidable, leakage pathway areas of the parenchyma.

Further work is required to understand how these observations may be translated to acute and chronic infusions in the human diseased brain. The challenge to clinicians utilising CED systems remains the integration of current knowledge of surgical planning techniques and the integration of expensive real-time imaging for the benefit of long term optimisation of target coverage.

Continued investment in CED platforms is resulting in more robust designs being available for investigational and clinical trial use. Continued research to optimise acute and chronic CED devices, as well as their infusion regimes, is necessary to maximise the coverage of neuroanatomical structures and provide the best chance of success in neurodegenerative and neuro-oncological treatments and investigational studies. Development and use of similar devices pre-clinically and clinically is essential to translate the learning and experiences gained.

6 Acknowledgements

Special thanks go to the staff at the Translational Biomedical Research Centre, Bristol, UK.

7 References

Bankiewicz, K. S. et al. 2000. Convection-enhanced delivery of AAV vector in parkinsonian monkeys; in vivo detection of gene expression and restoration of dopaminergic function using pro-drug approach. *Exp Neurol* 164(1), pp. 2-14. doi: 10.1006/exnr.2000.7408

Bankiewicz, K. S. et al. 2016. AAV viral vector delivery to the brain by shape-conforming MR-guided infusions. *J Control Release* 240, pp. 434-442. doi: 10.1016/j.jconrel.2016.02.034

Bartus, R. T. et al. 2013. Advancing neurotrophic factors as treatments for age-related neurodegenerative diseases: developing and demonstrating "clinical proof-of-concept" for AAV-neurturin (CERE-120) in Parkinson's disease. *Neurobiol Aging* 34(1), pp. 35-61. doi: 10.1016/j.neurobiolaging.2012.07.018

Barua, N. U. et al. 2013a. Robot-guided convection-enhanced delivery of carboplatin for advanced brainstem glioma. *Acta Neurochir (Wien)* 155(8), pp. 1459-1465. doi: 10.1007/s00701-013-1700-6

Barua, N. U. et al. 2013b. Convection-enhanced delivery of AAV2 in white matter--a novel method for gene delivery to cerebral cortex. *J Neurosci Methods* 220(1), pp. 1-8. doi: 10.1016/j.jneumeth.2013.08.011

Barua, N. U. et al. 2013c. Intermittent convection-enhanced delivery to the brain through a novel transcutaneous bone-anchored port. *J Neurosci Methods* 214(2), pp. 223-232. doi: 10.1016/j.jneumeth.2013.02.007

Bienemann, A. et al. 2012. The development of an implantable catheter system for chronic or intermittent convection-enhanced delivery. *Journal of Neuroscience Methods* 203(2), pp. 284-291. doi: 10.1016/j.jneumeth.2011.10.002

Bobo, R. H. et al. 1994. Convection-enhanced delivery of macromolecules in the brain. *Proc Natl Acad Sci U S A* 91(6), pp. 2076-2080.

Brady, M. L. et al. 2013. Pathways of infusate loss during convection-enhanced delivery into the putamen nucleus. *Stereotact Funct Neurosurg* 91(2), pp. 69-78. doi: 10.1159/000342492

Breeze, R. E. et al. 1995. Implantation of fetal tissue for the management of Parkinson's disease: a technical note. *Neurosurgery* 36(5), pp. 1044-1047; discussion 1047-1048.

Chen, M. Y. et al. 1999. Variables affecting convection-enhanced delivery to the striatum: a systematic examination of rate of infusion, cannula size, infusate concentration, and tissue-cannula sealing time. *J Neurosurg* 90(2), pp. 315-320. doi: 10.3171/jns.1999.90.2.0315

Field, A. 2007. *Discovering statistics using SPSS : (and sex, drugs and rock 'n' roll)*. London: Sage.

Gill, S. S. et al. 2003. Direct brain infusion of glial cell line-derived neurotrophic factor in Parkinson disease. *Nat Med* 9(5), pp. 589-595. doi: 10.1038/nm850

Gill, T. et al. 2013. In vitro and in vivo testing of a novel recessed-step catheter for reflux-free convection-enhanced drug delivery to the brain. *J Neurosci Methods* 219(1), pp. 1-9. doi: 10.1016/j.jneumeth.2013.06.008

Goetz, C. G. et al. 2008. Placebo influences on dyskinesia in Parkinson's disease. *Mov Disord* 23(5), pp. 700-707. doi: 10.1002/mds.21897

Ivanchenko, O. et al. 2010. Experimental techniques for studying poroelasticity in brain phantom gels under high flow microinfusion. *J Biomech Eng* 132(5), p. 051008. doi: 10.1115/1.4001164

Krauze, M. T. et al. 2005. Reflux-free cannula for convection-enhanced high-speed delivery of therapeutic agents. *J Neurosurg* 103(5), pp. 923-929. doi: 10.3171/jns.2005.103.5.0923

Kunwar, S. et al. 2010. Phase III randomized trial of CED of IL13-PE38QQR vs Gliadel wafers for recurrent glioblastoma. *Neuro Oncol* 12(8), pp. 871-881. doi: 10.1093/neuonc/nop054

Lang, A. E. et al. 2006. Randomized controlled trial of intraputamenal glial cell line-derived neurotrophic factor infusion in Parkinson disease. *Ann Neurol* 59(3), pp. 459-466. doi: 10.1002/ana.20737

Lewis, O. 2015. A systems based approach to drug delivery - a method that works. In: Woolley, M. et al. eds. *SNO-SCIDOT Joint Conference on Therapeutic Delivery to the CNS.* San Antonio, Texas, USA.

Lewis, O. et al. 2016. Chronic, intermittent convection-enhanced delivery devices. *J Neurosci Methods* 259, pp. 47-56. doi: 10.1016/j.jneumeth.2015.11.008

Mueller, S. et al. 2011. Effect of imaging and catheter characteristics on clinical outcome for patients in the PRECISE study. *J Neurooncol* 101(2), pp. 267-277. doi: 10.1007/s11060-010-0255-0

Raghavan, R. et al. 2016. Delivering therapy to target: improving the odds for successful drug development. *Ther Deliv* 7(7), pp. 457-481. doi: 10.4155/tde-2016-0016

Roitbak, T. and Sykova, E. 1999. Diffusion barriers evoked in the rat cortex by reactive astrogliosis. *Glia* 28(1), pp. 40-48.

Saltzman, W. M. 2001. *Drug delivery : engineering principles for drug therapy*. Oxford [England]; New York: Oxford University Press.

Sillay, K. et al. 2013. Strategies for the delivery of multiple collinear infusion clouds in convection-enhanced delivery in the treatment of Parkinson's disease. *Stereotact Funct Neurosurg* 91(3), pp. 153-161. doi: 10.1159/000345270

Singleton, W. G. B. et al. eds. 2017. *Development of new CED devices*. *SCIDOT-SNO.* San Francisco, USA,

Stockwell, J. et al. 2013. Novel Central Nervous System Drug Delivery Systems. *Chem Biol Drug Des*, doi: 10.1111/cbdd.12268

Warren Olanow, C. et al. 2015. Gene delivery of neurturin to putamen and substantia nigra in Parkinson disease: A double-blind, randomized, controlled trial. *Ann Neurol* 78(2), pp. 248-257. doi: 10.1002/ana.24436

White, E. et al. 2011. A robust MRI-compatible system to facilitate highly accurate stereotactic administration of therapeutic agents to targets within the brain of a large animal model. *Journal of Neuroscience Methods* 195(1), pp. 78-87. doi: 10.1016/j.jneumeth.2010.10.023

Woolley, M. et al. eds. 2013. *Factors Facilitating Optimised Intraparenchymal Drug Delivery – A Prescriptive Systems Approach*. *Partnership Opportunities in Drug Delivery.* Boston, USA,

Yin, D. et al. 2009. Striatal volume differences between non-human and human primates. *J Neurosci Methods* 176(2), pp. 200-205. doi: 10.1016/j.jneumeth.2008.08.027